ВЫСОКОМОЛЕКУЛЯРНЫЕ СОЕДИНЕНИЯ, Серия А, 2011, том 53, № 5, с. 681–690

СТРУКТУРА И СВОЙСТВА

УДК 541.64:536.6

HEAT CAPACITY AND VIBRATIONAL DYNAMICS OF POLYVINYLIDENE FLUORIDE (β-FORM)[1]

© 2011 г. Archana Gupta[a], Parag Agarwal[a], Saba Bee[a], Poonam Tandon[b], and V. D. Gupta[b]

[a] *Department of Applied Physics, Institute of Engineering and Technology, M.J.P. Rohilkhand University, Bareilly, India*

[b] *Department of Physics, Lucknow University, Lucknow, India*

e-mail: drarchana.physics@gmail.com

Received October 18, 2010
Revised Manuscript Received December 28, 2010

Abstract—Polyvinylidene fluoride (PVDF) is a polymer of industrial importance, mainly due to its piezoelectric and pyroelectric properties. A comprehensive study of the normal modes and their dispersion in PVDF (β-form) has been reported in the reduced zone scheme using Wilson's *GF* matrix method as modified by Higgs. A Urey–Bradley force field has been used. The evaluation of normal modes and their dispersion has been taken to logical conclusion by calculating the heat capacity as a function of temperature. The extent of agreement with the experimental data supports the potential field. Characteristic features of the dispersion curves such as repulsion and exchange of character have also been discussed.

INTRODUCTION

Polyvinylidene fluoride (PVDF) is a chemically inert but electronically active thermoplastic polymer. It has a variety of applications [1–8]. It is commonly used in chemical, medical and defense industries. The piezoelectric and pyroelectric responses of PVDF rival those of ceramics. Lower cost, large area, flexibility, and low acoustic impedance are among the advantages of PVDF over ceramics due to its polymeric nature. Strong piezoelectric properties, stability to UV radiation and high continuous-use temperature make PVDF suitable for various IR integrated optics applications [5]. The cylindrical microlenses and microlens arrays can be fabricated by CO_2 laser irradiation of polyvinylidene fluoride substrate. The natural flame retardancy and flexibility of PVDF leads to many uses in the jacketing of fiber optic cables, fiber optic raceways and copper cable used in plenum areas of buildings. The mechanical properties and cytotoxicity (biocompatibility) of polyvinylidene fluoride and hydroxyapatite (HAP) composites are used in bone restoration and filling [6]. Microfabricated piezoelectric PVDF structures could find applications in the fabrication of mechanically active tissue engineering scaffolds, and the development of dynamic sensors at the cellular and subcellular levels. Polymer electrolytes based on polyvinylidene fluoride have wide applications in lithium batteries and proton fuel cells [7].

The chemical structure of PVDF ($-CH_2-CF_2-$), intermediate between polyethylene and polytetrafluoroethylene, gives the polymer chain both flexibility and some stereo-chemical constraints. Consequently, PVDF exhibits polymorphism with at least five phases found experimentally depending on the crystallization temperature, mechanical stress, casting solvent, electric field and other crystallization conditions [9]. Five crystal phases with different conformations are all-trans (ttt) planar zig-zag β-phase, tgtg' (g denotes gauche form) α- and δ-phases, and t_3gt_3g' γ- and ε-phases [10, 11]. Since the C–F bond is a polar bond, different phases of PVDF possess different amount of net dipole moment. The β-phase has the highest dipole moment per unit, as in this conformation all the diploes are aligned in the same direction [12]. In the cases of polar β-, γ- and δ-phases, the polymer chains pack into crystals with parallel dipoles, hence the crystal possesses a net dipole moment whereas, in the cases of non-polar α- and ε-phases, they do with anti-parallel dipoles hence the net dipole moment vanishes. Among these phases, the β-phase has the highest spontaneous polarization in a unit crystal cell [13]. The large value of unit cell polarization for an oriented and polarized sample is from the closer packing of polymer chains in a unit cell. Therefore, the polar β-phase has attracted technological interest.

FTIR spectroscopy is a major technique for investigating polymer sample in terms of composition as well as constituents' distribution. Apart from different chemical distributions in the sample, the spectroscopist is also able to visualize areas with different degree of crystallinity or preferred orientation and by these means ensure reliable data about the quality of the investigated sample, manufacturing process, etc. Raman spectroscopy is a nondestructive analytical technique and is complementary in nature to infrared spectroscopy. This can provide information from functional groups with vibration modes that are weak or unresolvable by FTIR. Normal mode analysis helps in pre-

[1] Статья печатается в представленном авторами виде.

cise assignments and identification of spectral features of a molecule of known structure and force field. In general, the IR absorption, Raman spectra from polymeric systems are very complex and cannot be unraveled without the full knowledge of dispersion curves. One cannot appreciate the origin of both symmetry dependent and symmetry independent spectral features without the knowledge of dispersion curves. The dispersion curves also facilitate correlation of the microscopic behavior of the long chain molecule with the macroscopic properties such as entropy, enthalpy, specific heat etc. In continuation of our work on normal coordinate analysis and phonon dispersion in a variety of polymers in different conformations [14–17], we present here a complete normal mode analysis of PVDF (β-form) with phonon dispersion in the first Brillouin zone using the Urey–Bradley force field (UBFF) [18].

The infrared and Raman spectra of PVDF have been studied by many workers [19–22], however, these studies suffer from one or the other infirmities. Enomoto et al. [19] have reported limited studies on the vibrational spectrum of PVDF. They have worked out the spectra of the polymeric form without introducing phase factor between successive units. Boerio and Koenig [20] have performed normal mode analysis using valence force field that does not take into account non-bonded interactions in both gem and tetra positions and tension terms. They have also not reported the dispersive behavior of the polymer. Lack of information on the dispersive behavior of normal modes in many polymeric systems has been responsible for incomplete understanding of polymeric spectra. The study reported by Wang et al. [21] using DFT is focused mainly on piezoelectric behavior. They simulated the vibrational spectra, which is limited only to zone center frequencies, and in practice, there are absorption bands beyond the zone center. The problem of PVDF has been attempted by Tadokoro et al. [22] also. They have considered the crystalline form and evaluated the dispersion curves. This is a difficult problem because of the large number of interactions involved, which are even difficult to visualize. Even the physical dimensions of the secular equation become intractable. Since they have used valence force field, which takes into account only limited interactions, it is very difficult to comment on its veracity. Normally one starts with a full solution for an isolated chain, which broadly gives profile of the dispersion curves as least for weak interactions. A transition from linear chain to crystalline form only results in splitting at the zone centre and zone boundaries depending on the crystal field symmetry as reported by neutron inelastic and coherent scattering [23]. These are a couple of other things, which have to be checked for a three-dimensional system, e.g., the regions of high density-of-states (von-Hove type singularities) in the dispersion curves should be reflected in additional absorption bands in Raman or IR spectra. There should be many more absorption bands in Raman or IR spectra because of the presence of regions of high density-of-states in the dispersion curves reported by Tadokoro et al. [22]. Their absence does not support the three-dimensional model used by them. In addition to the above, we feel that for detailed spectroscopic and dynamic study of macromolecules, a force field is required that not only predicts structures and thermodynamic quantities but also reliably reproduces data to spectroscopic standards, i.e., vibrational frequencies. The Urey–Bradley force field (UBFF) used by us has certain advantages over the valence force field: (1) Relatively less number of parameters are required to express the potential energy. (2) No quadratic cross terms are included in the potential energy expression. (3) The force constants are supplemented by the repulsive forces between non-bonded atoms, which simulate the van der Waals force between them. It gives a better description of intra and inter unit interactions and arbitrariness in choosing the force constants is reduced, thereby enabling us to arrive at a better force field. In view of the above, it was felt necessary to have a re-look at the dispersive behavior of a linear chain of PVDF, particularly van Hove type singularities, which give rise to additional absorption bands, which also affect thermodynamic behavior. We have also calculated the values of heat capacity in the range 10–210 K and matched with the experimental values obtained from ATHAS data bank reported by Wunderlich et al. [24]. To the best of our knowledge, such detailed studies leading to correlation between the microscopic behavior and macroscopic properties of this polymer have not yet been reported.

THEORY

Calculation of Normal Mode Frequencies

The calculation of normal frequencies has been carried out according to Wilson's *GF* matrix method [25] as modified by Higg's [26] for an infinite chain. This method consists of writing inverse kinetic energy matrix *G* and the potential energy matrix *F* in terms of internal coordinates *R*. In the case of an infinite isolated helical polymer, there are an infinite number of internal coordinates, which lead to *G* and *F* matrices of infinite order. Due to the screw symmetry of the polymer, a transformation similar to that given by Born and Von Karman can be performed which reduces the infinite problem to finite dimensions.

The transformation consists of defining a set of symmetry coordinates

$$S(\delta) = \sum_{s=-\infty}^{\infty} R^n \exp(is\delta),$$

where δ is the vibrational phase difference between the corresponding modes of the adjacent residue units.

The elements of the $G(\delta)$ and the $F(\delta)$ matrices have the form

$$G_{ik}(\delta) = \sum_{s=-\infty}^{\infty} G_{ik}^{s} \exp(is\delta)$$

$$F_{ik}(\delta) = \sum_{s=-\infty}^{\infty} F_{ik}^{s} \exp(is\delta)$$

For any given phase difference δ (other than 0 or π), the $G(\delta)$ and the $F(\delta)$ matrices are complex. In order to avoid the difficulties involved in handling complex numbers, methods have been devised to transform the complex matrices into equivalent real matrices by constructing suitable linear combinations of the coordinates. One method of transforming a complex matrix to its real matrix equivalent is through a similarity transformation. It can be shown that any complex matrix $H = M + iN$ can be replaced by the real one

$$\begin{pmatrix} M & -N \\ N & M \end{pmatrix}$$

In the present case, we can write $G(\delta) = G^R(\delta) + iG^I(\delta)$ and $F(\delta) = F^R(\delta) + iF^I(\delta)$, where $G^R(\delta)$, $F^R(\delta)$, $G^I(\delta)$, $F^I(\delta)$ are real and imaginary parts of $G(\delta)$ and $F(\delta)$.

The product $H(\delta) = G(\delta)\,F(\delta)$ becomes:

$$H(\delta) = \begin{pmatrix} G^R(\delta) & -G^I(\delta) \\ G^I(\delta) & G^R(\delta) \end{pmatrix} \times \begin{pmatrix} F^R(\delta) & -F^I(\delta) \\ F^I(\delta) & F^R(\delta) \end{pmatrix} = \begin{pmatrix} H^R(\delta) & -H^I(\delta) \\ H^I(\delta) & H^R(\delta) \end{pmatrix},$$

where

$$H^R(\delta) = G^R(\delta)F^R(\delta) - G^I(\delta)F^I(\delta)$$

$$H^I(\delta) = G^R(\delta)F^I(\delta) + G^I(\delta)F^R(\delta)$$

The matrix $H(\delta)$ now has dimensions $2N \times 2N$. The eigenvalues therefore occur in pairs of equal values. The difficulty of dealing with complex numbers is thus avoided.

The vibrational secular equation that gives normal mode frequencies and their dispersion as a function of phase angles has the form

$$|G(\delta)F(\delta) - \lambda(\delta)I| = 0 \quad 0 \le \delta \le \pi \tag{1}$$

The vibration frequencies $\nu(\delta)$ (in cm^{-1}) are related to the eigen values $\lambda(\delta)$ by the following relation:

$$\lambda(\delta) = 4\pi^2 c^2 \nu^2(\delta) \tag{2}$$

Potential energy for the Urey–Bradley force field used in the present work can be written as

$$V = \sum K_{j,k} r_{j,k}^{(m)} \left(\Delta r_{j,k}^{(m)}\right) + K_{j,k}\left(\Delta r_{j,k}^{(m)}\right)^2/2 + \sum H'_{i,j,k} r_{i,j}^{(m)} r_{j,k}^{(m)} (\Delta\alpha_{i.j.k}^{(m)}) + F_{i,k}\left(\Delta q_{i,k}^{(m)}\right)^2/2 + \sum K_j^{\tau}(\Delta\tau_j)^2 + \sum K_j^{\omega}(\Delta\omega_j)^2, \tag{3}$$

where the symbols have their usual meanings. The primed quantities are introduced as internal tensions. Non-bonded interactions involve attraction and repulsion of atoms due to nth overlap of their electron shells. These effects are usually expressed by the 6-exp or 6–12 type potentials. The tension terms are assumed zero.

Force Constant Evaluation

The force constants were obtained by the least square fitting. In order to obtain the "best fit" with the observed frequencies, the following procedure was adopted. Initially, approximate force constants were transferred from polyethylene [27] and those related to fluorine by polytetrafluoroethylene [28]. Thus, starting with the approximate F matrix F_0 and the observed frequencies λ_{obs} (related through a constant), one can solve the secular matrix equation:

$$GF_0L_0 = L_0\lambda_0 \tag{4}$$

Let $\Delta\lambda_i = \lambda_{iobs} - \lambda_{io}$ in the above equation, it can be shown that in the first order approximation

$$\Delta\lambda = j\Delta F,$$

where j is computed from L_0.We wish to compute the corrections to F_0 so that the errors $\Delta\lambda$ are minimized. We use the theory of least square and calculate

$$j'p\Delta\lambda = (j'pj)\Delta F, \tag{5}$$

where p is a weighting matrix and j' is the transpose of j. The solution to this equation is obtained by inverting $(j'pj)$ to give

$$\Delta F = (jpj)^{-1} jp\Delta\lambda \tag{6}$$

If the number of frequencies is greater than the number of matrix elements, the matrix $j'pj$ should be nonsingular and we obtain the correction ΔF, which will minimize the sum of weighted squares of the residuals. If the corrections ΔF are fairly large, the linear relation between force constant and frequency term in the matrix Eq. (4) breaks down. In such a situation, further refinement using higher order terms in Taylor's series expansion of $\Delta\lambda_i$ is needed. This procedure was developed by Kings and others [29].

Calculation of Heat Capacity

Dispersion curves can be used to calculate the specific heat of a system. For a one-dimensional system, the density of state function or the frequency distribution function expresses the way energy is distributed among the various branches of normal modes in the crystal. It is calculated from the relation

$$g(\nu) = \sum [(\partial\nu_j/\partial\delta)^{-1}]_{\nu j(\delta)=\nu j} \tag{7}$$

The sum is over all the branches j. If we consider a solid as an assembly of harmonic oscillators, the frequency distribution $g(\nu)$ is equivalent to a partition function. The constant volume heat capacity can be calculated using Debye's relation

$$C_v = \sum g(\nu_j) k N_A (h\nu_j/kT)^2 \times [\exp(h\nu_j/kT)/\{\exp(h\nu_j/kT) - 1\}^2] \tag{8}$$

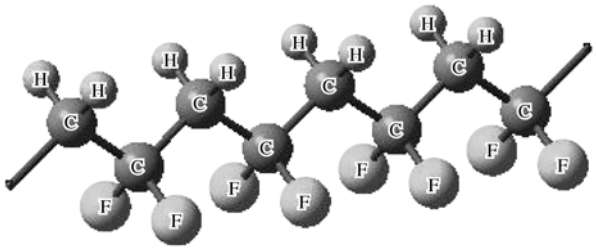

Fig. 1. Chain structure of PVDF (β-form).

with $g(\nu_i)d\nu_i = 1$.

The constant volume heat capacity C_v, given by Eq. (7) is converted into constant pressure heat capacity C_p using the Nernst–Lindemann approximation

$$C_p - C_v = 3RA^0(C_p^2 T/C_v T_m), \quad (9)$$

where A^0 is a constant, having value 3.9×10^{-3} K Mol/J and T_m is the estimated equilibrium melting temperature, 483 K in this case.

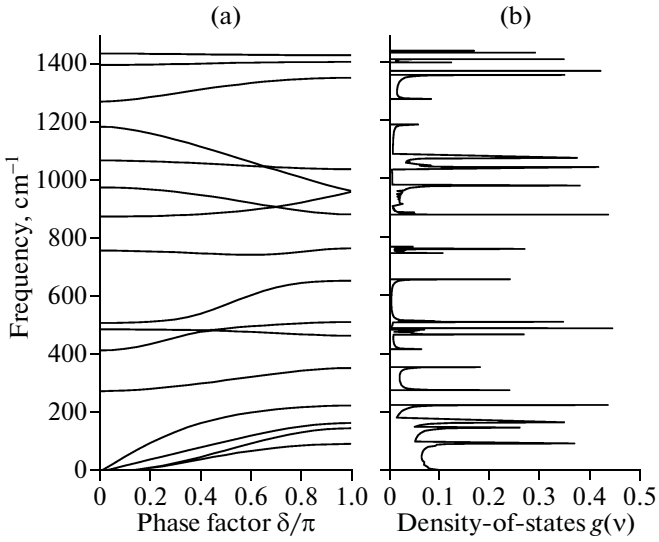

Fig. 2. (a) Dispersion curves of PVDF (0–1500 cm^{-1}), (b) density-of-states of PVDF (0–1500 cm^{-1}).

RESULTS AND DISCUSSION

PVDF (β-form) has an orthorhombic crystal structure with space group Cm2m-C_{2v} having lattice constants a = 8.58 Å, b = 4.91 Å and c (fiber axis) = = 2.56 Å [22]. There are six atoms in one repeat unit of PVDF (–CH_2–CF_2–) (Fig. 1) which give rise to 14 optically active vibrations of non-zero frequencies. The four modes for which $\omega \to 0$ as $\delta \to 0$ are called acoustic modes. They are due to translation (one parallel and two perpendiculars to the chain axis) and one due to rotation around the chain axis.

The vibrational frequencies were calculated from the secular equation [1] for values of δ varying from 0 to π in steps of 0.05π. Initially approximate force constants were taken from the potential field data of polyethylene [27] and those involving fluorine atoms from polytetrafluoroethylene [28]. These were later refined to give the "best fit" to the observed IR and Raman spectra [22, 30]. We have used the Urey–Bradley force field. The assignments were made on the basis of potential energy distribution (PED), band shape, band intensity and appearance/disappearance of modes in similar molecular groups placed in similar environment. The final force constants along with the internal coordinates are given in Table 1. There is a wide difference in the force constants used by earlier workers [20, 22] and the present one. This is much too obvious because the Urey–Bradley force field covers a wide potential surface including non-bonded interactions and tension terms. This is widely reflected in the off-diagonal elements of F-matrix and the profile of the dispersion curves. The matched frequencies along with their potential energy distribution (PED) are given in Table 2.

Table 1. Internal coordinate and Urey–Bradley force constants

Internal coordinates	Force constants
ν[C–H]	4.50
ν[C–C]	1.87
ν[C–F]	3.12
ϕ[H–C–C]	0.54(0.30)
ϕ[H–C–H]	0.36(0.28)
ϕ[C–C–F]	0.48(0.64)
ϕ[C–C–C]	0.30(0.20)
ϕ[F–C–F]	0.75(0.90)
τ[C–C]	0.034

Note: 1. ν, ϕ and τ denote stretch, angle bend and torsion, respectively.
2. Non-bonded force constants are given in parentheses.
3. Unit of force constants for stretch is md/Å, for angle bend is md/Å rad^{-2} and for torsion is mdÅ.

The dispersion curves are plotted in Fig. 2a from 0 to 1500 cm^{-1}. Since all the modes above 1500 cm^{-1} are non-dispersive in nature, the dispersion curves are plotted only for the modes below 1500 cm^{-1}. For the sake of simplicity, the modes are discussed under three heads: CH_2 modes, CF_2 modes and skeletal modes. All the modes of CH_2 and CF_2 have been confirmed by L-vector analysis.

CH_2 Modes

The CH_2 asymmetric and symmetric stretches calculated at 3020 and 2984 cm^{-1} match well with the observed frequencies at 3022, 2980 cm^{-1} in IR and 3020, 2984 cm^{-1} in Raman spectra. These are highly local-

Table 2. Normal modes and their dispersions in PVDF

Calc. Freq.	Obsd. Freq.			Assignment ($\delta = 0$) % PED	Calc. Freq.	Obsd. Freq.			Assignment ($\delta = \pi$) % PED
	IR[a]	Raman[a]	IR[b]			IR[a]	Raman[a]	IR[b]	
2984*	2980	2984	–	ν[C–H] (100)					
3020*	3022	3020	–	ν[C–H] (100)					
1436	1428	1435	1431	ϕ[H–C–H] (73) + ϕ[H–C–C] (25)	1430	1428	1435	1431	ϕ[H–C–H] (69) + ϕ[H–C–C] (25)
1397	1398	1400	1406	ϕ[H–C–C] (85) + ν[C–C] (15)	1408	1398	1400	1406	ϕ[H–C–C] (87)
1271	1273	1274	1279	ϕ[H–C–C] (96)	1354	1273	1274	1279	ϕ[H–C–C] (80) + ν[C–F] (13)
1185	1176	1180	1172	ν[C–F] (40) + ϕ[H–C–C] (37) + ϕ[C–C–F] (21)	1039	1176	1180	1172	ν[C–F] (34) + ν[C–C] (48)
1070	1071	1070	1074	ν[C–F] (33) + ν[C–C] (33) + ϕ[F–C–F] (15) + ϕ[C–C–C] (16)	964	1071	1070	1074	ν[C–F] (56) + ϕ[H–C–C] (25) + ϕ[C–C–F] (11)
976	–	980	–	ν[C–C] (73) + ϕ[C–C–F] (24)	961	–	980	–	ϕ[H–C–C] (53) + ν[C–F] (29) + ϕ[C–C–F] (10) + τ[C–C] (6)
877	884	885	881	ν[C–F] (59)+ ϕ[H–C–C] (27) + τ[C–C] (12)	884	884	885	881	ν[C–C] (77) + ϕ[C–C–F] (22)
760	840	845	841	ν[C–F] (59) + ν[C–C] (22) + ϕ[C–C–C] (10)	768	840	845	841	ν[C–F] (55) + ν[C–C] (32)
511	508	514	511	ϕ[F–C–F] (77) + ϕ[C–C–F] (17)	656	508	514	511	ϕ[C–C–F] (62) + ϕ[C–C–C] (22)
489	468	475	469	ϕ[C–C–F] (69) + τ[C–C] (22) + ν[C–F] (7)	515	468	475	469	ϕ[F–C–F] (78) + ϕ[C–C–C] (10)
417	442	445	441	ϕ[C–C–F] (90)	468	442	445	441	ϕ[C–C–F] (76) + τ[C–C] (23)
277	–	268	–	ϕ[C–C–F] (97)	357	–	268	–	ϕ[C–C–F] (92) + ν[C–F] (7)

Note: 1. All frequencies are in cm^{-1}.
2. [a] and [b] marked frequencies have been taken from Refs. [22] and [30], respectively.
3. The PED's of * marked frequencies are given only at the zone center because these frequencies are non-dispersive in nature.
4. Only dominant PED's are given.

Table 3. Comparison of CH_2 modes of PVDF, PVDC and PE

CH_2 modes	PVDF[a]	PVDC[b]	PE[c]
Asymmetric stretch	3022	2982	2883
			2919*
Symmetric stretch	2980	2947	2848
			2851*
Scissoring	1428	1403, 1358	1416
			1473*
Wagging	1398	1409, 1403, 1358	1175
			1370*
Twisting	1273	1265, 1180	1050
			1296*
Rocking	1176, 884	980, 752	1170
			734*

Note: 1. All frequencies are in cm^{-1}.
2. [a], [b] and [c] marked frequencies are taken from Refs. [22], [33] and [27], respectively.
3. Unmarked and * marked frequencies correspond to zone centre and zone boundary, respectively.
4. PVDF – Polyvinylidene fluoride, PVDC – Polyvinylidene chloride, PE – Polyethylene.

ized modes and hence non-dispersive in nature. The CH_2 scissoring mode is calculated at 1436 cm^{-1} and is assigned to the peak observed at 1428/1435 cm^{-1} in the IR/ Raman spectra. This mode also, does not couple with others and hence non-dispersive. The mode observed at 1398 cm^{-1} in IR has major contribution from CH_2 wagging. This mode has a small contribution from C–C stretching also and is in agreement with the assignment made by earlier workers [20, 22]. The mode observed at 1273 cm^{-1} in IR has been assigned to C–F and C–C stretching by Tadokoro et al. [22] and to C–F stretching, CF_2 rocking by Boerio and Koenig [20]. Our calculations show that this is a CH_2 twisting mode, which is in the same range as in other polymers shown in Table 3. Our assignment has further support by the fact that the C–F stretching vibrations occur in the frequency region about 1050 cm^{-1} [31]. The modes calculated at 1185 and 877 cm^{-1} consists of CH_2 rocking, which is in the usual range. In both these modes, C–F stretching is mixed with CH_2 rocking.

It is interesting to compare the CH_2 modes in polyethylene (PE) [32] and other halide derivatives of polyethylene, i.e., polyvinylidenefloride (PVDF) and polyvinylidenechloride (PVDC) [33] (Table 3). In PE, the CH_2 group is placed between two identical groups whereas in PVDF it is sandwiched between two CF_2 groups. The latter provides a much stronger interaction and hence, as expected, the frequencies of CH_2 group modes appear higher in PVDF than in PE. Similar trend is seen in case of PVDC also (except for wagging). This difference could be due to PVDC going into helical structure.

CF_2 Modes

The C–F asymmetric and symmetric stretching is calculated at 1185, 877 cm^{-1} and 1070, 760 cm^{-1}, respectively. The intense peaks at 1176, 884 cm^{-1} and 1071, 840 cm^{-1} in IR [22] are assigned to these vibrations. The stretching vibrations of carbon-fluorine, which is highly polar bond give strong intensity in infrared spectra as the IR is associated with the change in permanent dipole moment. On the contrary, the Raman lines are less intense as they are governed by changes in induced dipole moment during vibrations [34]. The CF_2 stretching vibrations are strongly coupled in contrast to the CH_2 stretching vibrations. This coupling takes away the group character of these frequencies and adds to the dispersive behavior. The same is evident from the PED given in Table 2. In addition to the C–F stretching, the CF_2 deformation modes are also highly coupled and these dominate in the lower frequency range. The mode calculated at 511 cm^{-1} is assigned to CF_2 scissoring and is in agreement with other authors [20, 22]. This mode exhibits the largest dispersion of 145 wave numbers. The CF_2 rocking and wagging modes are calculated at 489, 417 cm^{-1}, respectively, and are assigned to the peaks at 468, 442 cm^{-1} in IR. These two peaks are characteristic of β-chain as in case of α-phase a single peak of medium intensity is found at 490 cm^{-1} [21]. A comparison of the CH_2 and CF_2 modes in α- [35] and β-form of PVDF is given in Table 4. The CF_2 twisting mode calculated at 277 cm^{-1} is assigned to peak observed at 268 cm^{-1} in the Raman spectra. It shows a large dispersion of 80 wave numbers, reaching 357 cm^{-1} at the zone boundary. Table 5 shows the growing tendency of increased coupling on increasing fluorine substitution and this effect is reflected in the dispersion curves of PTFE [28].

Skeletal Modes

The modes that involve the motion of the backbone atoms are termed as skeletal modes. The mode calculated at 976 cm^{-1} corresponds to the peak observed at 980 cm^{-1} in the Raman spectra. It has major contribution from skeletal stretches and a small contribution from CF_2 wagging. Boerio and Koenig [20] and Tadokoro et al. [22] have assigned this mode to CH_2 twisting. On observing the dispersive behavior of this mode, we see that at $\delta = 0.70\pi$, this mode exchanges character with the mode at 877 cm^{-1} consisting of C–F stretching and CH_2 rocking. After the exchange of character, this has contribution from CH_2 rocking. Interestingly it is analyzed through L-vector analysis that the rocking character of this mode is converted into twisting one at $\delta = 0.75\pi$. The character of this mode remains twisting until the zone boundary. This explains the assignment made by other authors [20, 22]

to twisting mode. Other skeletal stretch modes are calculated at 1070 and 760 cm^{-1}. In both these modes, skeletal stretch C–C and skeletal bending C–C–C is present along with the C–F stretching. The backbone torsion appears in modes at 877 and 489 cm^{-1}. All these modes are highly coupled mixed modes and show appreciable dispersion.

Characteristic Features of the Dispersion Curves

Dispersion curves provide knowledge of the degree of coupling and information concerning the dependence of the frequency of a given mode on the sequence length of ordered conformations. Thus, the study of phonon dispersion in polymeric systems is an important study. The CH_2 twisting mode at 1271 cm^{-1} shows a large dispersion of 83 wave numbers. As phase factor δ increases, the contribution of twisting decreases slowly whereas that of C–F stretching comes in. The mode at 1185 cm^{-1} consists of C–F stretch, CH_2 rocking and CF_2 rocking. Both these modes diverge from each other right at the zone centre. Such a divergence is generally the result of repulsive coupling. This widens the PED within the entire zone in the diverging modes. The mode at 1185 cm^{-1}, as it progresses in the Brillouin zone suffers a repulsion at $\delta = 0.65\pi$ with the zone centre mode at 1069 cm^{-1}. As usual, it undergoes an exchange of character at the repulsion point. In this case, it was difficult to decide whether there is a crossing or repulsion. For this, calculations at very close intervals of $\delta = 0.001\pi$ have been performed and the change in potential energy was closely watched. This combined with symmetry considerations confirmed that they were indeed repulsions not crossings over. On the basis of quasi particle-particle scattering, this phenomenon of exchange of character may be viewed as a collision of two quasi particles in the energy momentum space, approaching each other and moving apart after exchanging their energies. This special characteristic of dispersion curves, repulsion and exchange of character is seen in other pair of modes also viz. modes at 1185, 1070 cm^{-1} and 976, 877 cm^{-1}. All such modes are listed in Table 6 along with their PED's before and after the exchange of character. No crossings are observed in the dispersion curves. The lower frequency modes are generally more sensitive to chain conformation and exhibit greater dispersion. The CF_2 scissoring mode at 511 cm^{-1} shows a large dispersion of 145 wave numbers. It has a little contribution of C–C–F bending and a trace of skeletal C–C–C bending also. This mode disperses a little initially but shows appreciable dispersion after $\delta = 0.40\pi$ beyond which the contribution of C–C–C bending starts increasing sharply. At the zone boundary, this contribution becomes 22%. With the advancement of δ, the contribution of scissoring decreases in this mode and shifts gradually to the mode at 417 cm^{-1} whereas the contribution of wagging in the mode at

Table 4. Comparison of CH_2 and CF_2 modes in α- and β-form of PVDF

CH_2/CF_2 modes	PVDF (β-form)[a]		PVDF (α-form)[b]	
	IR	Raman	IR	Raman
CH_2 Asymmetric stretch	3022	3030	3071	3072
			3068	3068
CH_2 Symmetric stretch	2980	2984	3016	3016
			3011	3010
CH_2 Scissoring	1428	1435	1407	1403
			1401	1402
			1353	1354
			1337	1342
CH_2 Wagging	1398	1400	1407	1403
			1401	1402
			1353	1454
			1337	1342
CH_2 Twisting	1273	1274	1004	1014
			913	913
CH_2 Rocking	1176	1180	831	829
	884	885	768	769
CF_2 Asymmetric stretch	1176	1180	1291	1294
			1254	1253
CF_2 Symmetric stretch	884	885	1151	1161
			1077	1078
CF_2 Scissoring	508	514	508	510
			465	464
CF_2 Wagging	442	445	465	464
			279	279
CF_2 Twisting	–	268	339	339
			279	279
CF_2 Rocking	468	475	392	392
			389	389

Note: 1. All frequencies are in cm^{-1}.
2. [a] and [b] marked frequencies have been taken from Refs. [22] and [35], respectively.

Table 5. Comparison of CF_2 modes of PVDF and PTFE

CF_2 modes	PVDF Cal. Freq. (cm^{-1})		PTFE* Cal. Freq. (cm^{-1})	
	$\delta = 0$	$\delta = \pi$	$\delta = 0$	$\delta = \pi$
Asym. stretch	1185	1039	1444	1230
Symm. stretch	1070	964	725	1155
Asym. stretch	877	884	1444	1230
Symm. stretch	760	768	725	1155
Scissoring	511	656	383	280
Rocking	489	515	527	300
Twisting	277	357	304	185

Note: 1. * Marked frequencies have been taken from Ref. [28].
2. PVDF – Polyvinylidene fluoride, PTFE – Polytetrafluoroethylene.

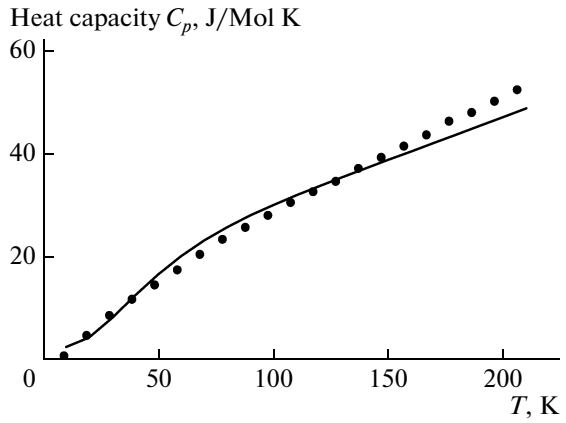

Fig. 3. Variation of heat capacity C_p with temperature: line represents calculated heat capacity, points represent experimental heat capacity.

417 cm^{-1} shifts to the upper mode in a gradual manner. This phenomenon continues until $\delta = 0.45\pi$ where the mode at 417 cm^{-1} suffers a repulsion and an exchange of character with the CF_2 rocking mode just above it (489 cm^{-1}). Another interesting phenomenon observed in the dispersion of CF_2 modes is seen in the CF_2 twisting mode at 277 cm^{-1}. At the point of repulsion and character exchange of the above-mentioned modes, the twisting mode also becomes a rocking mode whereas the wagging mode at 417 cm^{-1} at the zone centre becomes a twisting mode at the zone boundary. The character of these modes at different phase angles is listed in Table 7. To sum up, the foregoing discussion shows that the vibrational dynamics of an infinite system especially away from the zone centre and the zone boundary is a very complex phenomenon. The modes are not normal modes and are not controlled by symmetry. Their repulsive behavior, exchange of character etc. are difficult to analyze, much more so if the system is semi-crystalline in nature.

Frequency Distribution Function and Heat Capacity

Frequency distribution function has been obtained from the dispersion curves and plotted in Fig. 2b. The peaks in the frequency distribution curves correspond to the regions of high density of states (van Hove type singularities) [36]. These peaks compare well with the observed frequencies. The knowledge of density of states can be used to obtain the thermodynamic properties such as heat capacity, enthalpy etc. We have calculated the heat capacity of PVDF in the temperature range 10–210 K. K. Loufakis and B. Wunderlich [24] have reported experimental and theoretical heat capacity data for PVDF. The analysis is based on separation of the vibrational frequency spectrum into group and skeletal vibrations. The former are taken from computations fitted to IR and Raman data and the later by using the two parameter Tarasov model [24] and fitting to low temperature heat capacities. However, this approach has its own limitations, especially when the modes are strongly coupled. Separation of vibrational spectra into group and skeletal spectrum is justified only in the high frequency region where the modes are pure. Below 1200 cm^{-1} the modes get heavily mixed up as is evident from Table 2. Calculated heat capacity is shown in Fig. 3 by a continuous line and points represent the experimental data of PVDF.

Table 6. Characteristic features of dispersion curves

Pair of modes that repel and exchange character							
Freq. ($\delta = 0$)	(δ^a/π)	Before Exchange			After Exchange		
		(δ^b/π)	Freq.	% PED	(δ^b/π)	Freq.	% PED
1185	0.65	0.60	1064	ν[C–F] (35) + ϕ[C–C–H] (45) + ϕ[C–C–F] (15)	0.70	1046	ν[C–F] (35) + ν[C–C] (46) + ϕ[F–C–F] (14)
1069	0.65	0.60	1050	ν[C–F] (31) + ν[C–C] (44) + ϕ[F–C–F] (14)	0.70	1037	ν[C–F] (35) + ϕ[C–C–H] (45) + ϕ[C–C–F] (15)
976	0.70	0.65	916	ν[C–C] (70) + ϕ[C–C–F] (18)	0.75	917	ν[C–F] (49) + ϕ[C–C–H] (43) + ϕ[C–C–F] (15)
877	0.70	0.65	905	ν[C–F] (52) + ϕ[C–C–H] (34)	0.75	903	ν[C–C] (72) + ϕ[C–C–F] (19)
489	0.45	0.40	486	ϕ[C–C–F] (69) + τ[C–C] (23)	0.50	492	ϕ[F–C–F] (70) + ν[C–C] (12)
417	0.45	0.40	481	ϕ[F–C–F] (70) + ϕ[C–C–F] (25) + ν[C–C] (17)	0.50	484	ϕ[C–C–F] (70) + τ[C–C] (23)

Note: 1. All frequencies are in cm^{-1}.
2. Only dominant PEDs are given.
3. ^{a} corresponds to repulsion points.
4. ^{b} corresponds to points before/after repulsion.

Table 7. Character of CF_2 modes at different phase values

Normal mode frequencies (cm^{-1})	Character of CF_2 modes at $\delta/\pi =$								
	0.0	0.15	0.35	0.4	0.45	0.5	0.6	0.75	1.0
511	sciss.	sciss. + wagg.	wagg. + sciss.	wagg. + sciss.	wagg. + sciss.	wagg. + sciss.	wagg.	wagg.	wagg.
490	rock.	rock.	rock.	rock.	sciss. + wagg.	sciss. + wagg.	sciss.	sciss.	sciss.
417	wagg.	wagg.	wagg. + sciss.	sciss. + wagg.	rock.	rock.	rock.	twist.	twist.
277	twist.	twist.	twist.	twist.	rock.	rock.	rock.	rock.	rock.

The agreement obtained between the calculated values of the specific heat and the experimental measurements is reasonably good. A constant scaling factor of 1.707 has been used. This scaling factor takes into account the constant separation between the experimental and theoretical curves, which may arise from possible constant errors in the experimental measurements or in theory. Slight deviations could arise for two reasons, one the neglect of interchain interactions and other because of the force field being temperature independent. The former leads to lattice modes, which are of the same order of magnitude as the torsional modes. These are not included in the present model, and the heat capacity is sensitive to it. The evaluation of lattice modes is not only prohibitive dimensionally but also due to the enormity of interactions, which are difficult to visualize. As for the latter, the temperature dependence of force field is difficult to build in the potential field.

CONCLUSIONS

The Wilson's *GF* matrix method as modified by Higg's along with the Urey–Bradley force field has successfully explained the spectroscopic data on PVDF. The calculated values of heat capacity as a function of temperature within the range 10–210 K also agree with the experimental measurements reported by Wunderlich et al. [24]. It shows that the one-dimensional dynamics reasonably well explains the variation of heat capacity.

REFERENCES

1. A. G. Holmes-Siedle, P. D. Wilson, and A. P. Verrall, Material and Design **4 (6)**, 910 (1984).
2. T. R. Hay and J. L. Rose, IEEE transactions on Ultrasonics, Ferroelectrics, and Frequency Control **53 (6)**, 1212 (2006).
3. B. Lin and V. Giurgiutiu, Smart Mater. Struct. **15**, 1085 (2006).
4. D. H. Wang and S. L. Huang, J. Intell. Mater. Sys. and Struc. **11 (6)**, 482 (2000).
5. E. Bormashenko, R. Pogreb, Y. Socol, M. H. Itzhaq, V. Strelsov, S. Sutovski, A. Sheshnev, and Y. Bormashenko, Optic Materials **27 (3)**, 429 (2004).
6. F. J. C. Braga, S. O. Rogero, A. A. Couto, R. F. C. Marques, A. A. Ribeiro, and J. S. D. C. Campos, Mat. Res. **10 (3)**, 247 (2007).
7. E. Quartarone, P. Mustarelli, and A. Magistris, J. Phys. Chem. B **106 (42)**, 10828 (2002).
8. T. R. Hay and J. L. Rose, Sensors and Actuators A: Physical **100 (1)**, 18 (2002).
9. A. J. Lovinger, Science **220**, 1115 (1983).
10. A. J. Lovinger, Macromolecules **15**, 40 (1982).
11. M. G. Broahurst, G. T. Davis, J. E. McKinney, and R. E. Collins, J. Appl. Phys. **49 (10)**, 4992 (1978).
12. *E. Giannetti*, Poly. Inter. **50 (1)**, 10 (2001).
13. B. J. Jungnickel, in *Polymeric Materials Handbook*, Ed. Salamone J.C. (CRC Press Inc., New York, 1999), p. 7115.
14. D. Chaturvedi, S. Mishra, P. Tandon, V. D. Gupta, and H. W. Siesler, J. Polymer Eng. and Sci. **49**, 850 (2009).
15. A. Gupta, N. Choudhary, S. Bee, P. Tandon, and V. D. Gupta, Polymer Science Ser. A **52 (10)**, 1057 (2010).
16. N. Kumar, S. K. Shukla, P. Tandon, and V. D. Gupta, J. of Poly. Sci., Part B, Polymer Physics. **47,** 2353 (2009).
17. S. K. Shukla, N. Kumar, P. Tandon, and V. D. Gupta, J. Applied Polymer Sci. **116 (6)**, 3202 (2010).
18. H. C. Urey and C. A. Bradley, Phys. Rev. **38**, 1969 (1931).
19. S. Enomoto, Y. Kawai, and M. Sugita, J. Poly. Sci. Part **6 (A-2)**, 861 (1968).
20. F. J. Boerio and J. L. Koenig, J. Poly. Sci. **9 (A-2)**, 1517 (1971).
21. Z. Y. Wang, H. Q. Fan, K. H. Su, and Z. Y. Wen, Polymer **47**, 7988 (2006).
22. H. Tadokoro, M. Kobayashi, and K. Tashiro, Macromolecules **8 (2)**, 158 (1975).
23. L. A. Feldkamp, G. Venkateraman, and J. S. King, in *Proceedings of a Symposium on Neutron Inelastic Scattering Held at Copenhagen IAEA*, *Vienna 1968,* v. II, p. 159.
24. K. Loufakis and B. Wunderlich, Polymer **26**, 1875 (1985).
25. E. B. Wilson, J. C. Decius, and P. C. Cross, *Molecular Vibrations: The Theory of Infrared and Raman Vibrational Spectra* (Dover Publications, New York, 1980).
26. *P. W. Higg's*, Proc. Roy. Soc. (London) **A220**, 472 (1953).

27. A. Odajima and T. Maeda, J. Pol. Sci.: Part C **15,** 55 (1966).
28. M. J. Hannson, F. J. Boerio, and J. L. Koenig, J. Chem. Phys. **50(7)**, 2829 (1969).
29. W. T. Kings, I. M. Mills, and B. L. Crawford, J. Chem. Phys. **27***,* 455 (1957).
30. T. Baccaccio, A. Bottino, G. Capanneli, and P. Piaggio, J. Membrance Sci. **210,** 315 (2002).
31. C. N. Banwell and E. M. McCash, *Fundamental of Molecular Spectroscopy* (McGraw-Hill, New York, 1998).
32. V. Porwal, R. M. Mishra, P. Tandon, and V. D. Gupta, Ind. J. Biochem. Biophys. **41**, 34 (2004).
33. S. Gopal, *PhD Thesis* (University of Lucknow, Lucknow, India, 1996).
34. J. W. Hong, J. B. Lando, J. L. Koenig, S. H. Chough, and S. Krimm, Vibrational Spectroscopy **3**, 55 (1992).
33. N. J. Ramer, T. Marrone, and K. A. Stiso, Polymer **47**, 7160 (2006).
34. J. Callaway, *Quantum Theory of Solids* (Academic Press, New York and London, 1974).